Active platform stabilization with a 6D seismometer

Special Collection: Gravitational Wave Detectors

Amit Singh Ubhi ✉ iD ; Leonid Prokhorov iD ; Sam Cooper iD ; Chiara Di Fronzo iD ; John Bryant;
David Hoyland; Alexandra Mitchell iD ; Jesse van Dongen iD ; Conor Mow-Lowry iD ; Alan Cumming iD ;
Giles Hammond iD ; Denis Martynov iD

Check for updates

CrossMark

View Online

Export Citation

Articles You May Be Interested In

Seismometers as infrasound sensors

J Acoust Soc Am (October 2021)

Seismometer Sounds

J Acoust Soc Am (July 2005)

Teaching Geophysics with a Vertical-Component Seismometer

The Physics Teacher (December 2013)
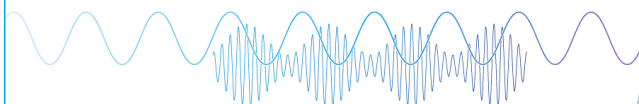
Active platform stabilization with a 6D seismometer

View Online   Export Citation   CrossMark

Amit Singh Ubhi,[1,a] (iD) Leonid Prokhorov,[1] (iD) Sam Cooper,[1] (iD) Chiara Di Fronzo,[1] (iD) John Bryant,[1] David Hoyland,[1] Alexandra Mitchell,[2,3] (iD) Jesse van Dongen,[2,3] (iD) Conor Mow-Lowry,[1,2,3] (iD) Alan Cumming,[4] (iD) Giles Hammond,[4] (iD) and Denis Martynov[1] (iD)

AFFILIATIONS

[1]Institute for Gravitational Wave Astronomy, School of Physics and Astronomy, University of Birmingham, Birmingham B15 2TT, United Kingdom
[2]Department of Physics and Astronomy, VU Amsterdam, Amsterdam 1081 HV, The Netherlands
[3]Dutch National Institute for Subatomic Physics, Nikhef, Amsterdam 1098 XG, Netherlands
[4]Institute for Gravitational Wave Research, School of Physics and Astronomy, University of Glasgow, Glasgow G12 8QQ, United Kingdom

Note: This paper is part of the APL Special Collection on Gravitational Wave Detectors.
a)Author to whom correspondence should be addressed: a.s.ubhi@bham.ac.uk

ABSTRACT

We demonstrate the control scheme of an active platform with a six degree of freedom (6D) seismometer. The inertial sensor simultaneously measures translational and tilt degrees of freedom of the platform and does not require any additional sensors for the stabilization. We show that a feedforward cancelation scheme can efficiently decouple tilt-to-horizontal coupling of the seismometer in the digital control scheme. We stabilize the platform in the frequency band from 250 mHz up to 10 Hz in the translational (X, Y) degrees of freedom and achieve a suppression factor of 100 around 1 Hz. Further suppression of ground vibrations was limited by the non-linear response of the piezo actuators of the platform and by its limited range (5 μm). In this paper, we discuss the 6D seismometer, its control scheme, and the limitations of the test bed.

The LIGO[1] and Virgo[2] detectors have made a number of gravitational wave detections from massive compact objects.[3–6] Sources of these waves range from two recent neutron star black hole systems[7] and binary black holes,[8–10] with one detection of an intermediate mass black hole of mass $\sim 150 M_\odot$.[10] A multimessenger event was also observed from a binary neutron star merger, which verified localization and decreased the false alarm rate of the detection.[11]

Low frequency sensitivity of the detectors determines the likelihood of observing more massive systems such as intermediate mass black hole binaries between 100 and $1000 M_\odot$ as well as providing early warning signals. The time until merger of binary systems scales with frequency as $f^{-8/3}$; therefore, low frequency noise improvements enable greater opportunities for multimessenger detections. For the LIGO detectors, these signals are cloaked by the non-stationary control noise of the isolation scheme of the core optics.[12–14] The LIGO isolation scheme consists of a four stage pendulum suspended from state of

the art two stage twelve axis platforms for the detectors' core optics.[15–17] Despite the orders of magnitude suppression achieved, the angular controls for the core optics limit the detectors' sensitivity below 30 Hz.[18,19]

Improved sensing of the isolated platforms would reduce the input motion to the suspension chain, reducing the injection of noise from the local damping on the optics. Suppression of platform tilt is limited by the lack of inertial rotation sensors on the platforms. The platform tilt also plagues the translational readout with an unfavorable coupling of g/ω^2,[20,21] where g is the local gravitational acceleration and ω is the angular frequency. Investigations into improved sensing of the platforms are being explored by a number of groups who develop inertial sensors. Krishna Venkateswara and the University of Washington group have employed the out of vacuum beam rotation sensor (BRS)[22,23] at LIGO for feedforward correction of translational sensors. The University of Washington is also developing an in
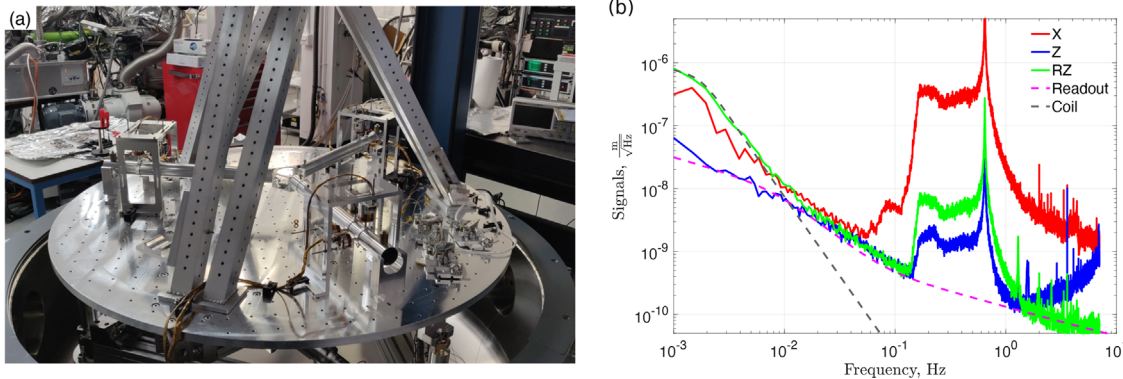
FIG. 1. (a) Photo of experimental setup. The round active platform is stabilized relative to the seismometer with three arms, and (b) an example of damped signals of the various degrees of freedom to highlight the noise floors due to sensing (readout) and damping (coil). Note that the Y and RX degrees of freedom are analogous to X and RY.

vacuum cylindrical rotation sensor (CRS). The University of Western Australia has developed the ALFRA rotational accelerometer, which has the advantage of multi-orientation such that it can also be mounted vertically.[24] Optical gyroscopes have also been investigated at Caltech and MIT, which make use of the Sagnac effect to measure the absolute rotation rate.[25,26] The commercial company blueSeis offers single axis and 3-axis fiber optic gyroscopes with guaranteed lifelong stability of <1%.[27] Further improvements to low noise translational inertial sensing have been demonstrated by the Nikhef and VU groups in Amsterdam,[28] and the Belgium China collaboration[29,30] with custom interferometric inertial sensors.

In this Letter, we present an initial version of the six degrees of freedom (6D) seismometer detailed in Ref. 31. The basis behind the design is a softly suspended extended reference mass, which is readout in six degrees of freedom (6D). Unlike the inertial sensors discussed above, the approach differs by utilizing a simple mechanical design, which enables cross couplings. Complexity is moved to the signal processing where the degrees of freedom must be untangled.

We demonstrate the viability of the device for use in feedback by stabilizing a rigid isolated platform in six degrees of freedom. First, we discuss the experimental design and then move through the control scheme, indicating the performance achieved and the shortcomings of the test bed used.

The seismometer consists of a single extended reference mass suspended from a fused silica fiber.[32,33] Optical shadow sensors known as Birmingham Optical Sensors and Electromagnetic Motors (BOSEMs)[34] were employed for the readout scheme, which measured the relative displacement between the proof mass and the platform. The test bed was a rigid stabilization platform, which was actuated using six piezo legs in a hexapod style formation. The experimental set up is shown in Fig. 1(a), and experimental parameters, highlighting the resonant frequencies of the proof mass, are summarized in Table I.

Ideally, the eigenmodes of the mass should be as low as possible to enable inertial sensing to lower frequencies. The stiffest degree of freedom in our setup is the vertical one, and the corresponding eigenfrequency of its bounce mode is 10 Hz. The other two translations degrees of freedom were softer with eigenmodes of 0.62 Hz. The eigenfrequencies were determined by the fiber length, which was constrained by the height of the vacuum chamber.

Resonant frequencies for the tilt modes (RX and RY) were tuned to 100 and 90 mHz by compensating the elastic restoring coefficient of the fiber with the gravitational anti-spring, respectively. The distance between the effective pivot point of the wire and the center of mass, d, enabled tuning of the effective restoring torque indicated as follows:[35]

$$\omega_{X}^{2} \approx \frac{g}{L}, \qquad \omega_{RY}^{2} \approx \frac{mgd + k_{el}}{I_y}, \qquad (1)$$

where m is the mass, k_{el} is the elastic restoring coefficient, and I_y is its moment of inertia about the y-axis.

The soft angular modes of the system result in large oscillations, which ringdown over extended periods of time. In particular, the ringdown time of the torsion mode (RZ) is several months. In order to maintain the BOSEM sensors within their linear regime, we implemented damping loops on the seismometer's resonant modes using coil–magnet pairs. The damping loops actuated directly on the mass in narrow frequency bands around its resonances and reduce the mass motion down to ~μm level.

Figure 1(b) shows the damped signals using the BOSEM actuation with no control of the platform. Large translational motion in X leaks into the other degrees of freedom, which can be seen from the presence of the microseism and resonant peak at 0.62 Hz. The reduction of the X (Y) platform motion diminishes this effect as the

TABLE I. A list of parameters and nominal values.

Parameters	Description	Value
m	Mass	1 kg
R	Mass radius	0.6 m
L	Fiber length	0.64 m
r	Fiber radius	$100 \pm 10 \, \mu$m
$f_{X,Y}$	Translational resonances	0.62 Hz
f_Z	Vertical resonance	10 Hz
f_{RX}	RX tilt resonance	100 mHz
f_{RY}	RY tilt resonance	90 mHz
f_{RZ}	RZ torsion resonance	2 mHz

platform tracks the motion of the proof mass. Experimental investigations into the BOSEM sensing and actuation noise found that the stiffest mode (Z) was limited by sensor noise below 10 Hz, and that the digital-to-analog converter noise from our control system dominates the RZ motion below 10 mHz.

For stable control of the actuated platform relative to the 6D seismometer, there were three key strategies that were implemented. The first two are regarding the 6D seismometer device, and the third is regarding the actuation problems that are relevant to the class of actuated platforms with cross couplings between different degrees of freedom on the level of $\approx 1\%$. First, diagonalization of the tilt modes of the proof mass. In the case of a symmetric fiber neck and mass, the circular cross section results in an infinite number of principle axes, resulting in no preferential axes around which the tilt motion occurs. This was initially assumed, and an arbitrary direction for the X and Y axes was chosen.

We discovered a discrepancy between the tilt resonances such that $f_{RX} \neq f_{RY}$. Investigations determined that asymmetry in the fiber neck, where bending occurs, gave rise to two perpendicular principal axes around which tilting occurred. The asymmetry resulted in non-identical elastic restoring constants, k_{el}, for RX and RY, where the frequency splitting of the modes was further exacerbated by the tunable gravitational restoring torque, mgd.

Measurement of the degrees of freedom was determined using an analytical sensing matrix determined by the system geometry, **S**. This converted the six BOSEM signals, $\vec{B}$, into the six degrees of freedom, $\vec{X}$, such that $\vec{X} = \mathbf{S}\vec{B}$. The preferential axes for tilt caused coupling of the RX eigenmode into the sensed RY motion (and RY to RX). Analysis of the individual BOSEM signals allowed us to determine the angular misalignment of our original axes compared to the principal axes due to the fiber asymmetry. A rotation matrix, **R**, was implemented to align the sensing with the eigenmodes of the principal axes, $\vec{X}_{eig}$, such that,

$$\vec{X}_{eig} = \mathbf{R}\vec{X} = \mathbf{R}\mathbf{S}\vec{B}. \qquad (2)$$

Similar to the sensing matrix, the platform actuation was set to align its principle rotation axis with the 6D seismometer.

The second key strategy was to decouple the horizontal-to-tilt motion of the proof mass. The platform causes movement of the suspension frame and the test mass, which is shown in Fig. 1(a). However, the test mass is considered to be inertial above the pendulum resonant frequencies. The coupling of platform motion, X_P and RY_P, to the sensor outputs, X and RY, can be written as

$$\begin{aligned} X &= T(f)X_P + L \times RY_P, \\ RY &= K(f)X_P + RY_P, \end{aligned} \qquad (3)$$

where L is the fiber length. X and RY and Y and RX are intrinsically coupled by the pendulum. Transfer functions $T(f)$ and $K(f)$ are determined by the pendulum and pitch resonances and are discussed in detail in Ref. 35.

According to Eq. (3), the coupling of X and RY and, similarly, Y and RX degrees of freedom is frequency dependent. Therefore, we implement a filter to diagonalize the degrees of freedom as shown in Fig. 2(a). We found that the control system requires the subtraction of X (Y) from RY (RX); hence, a 2×2 diagonalization is necessary for stability.

We determined the feedforward filter by solving Eq. (3) relative to X_P and RY_P. Since the solutions are given by the following equation:

$$\begin{aligned} X_P &= \frac{1}{T - LK}(X - L \times RY), \\ RY_P &= \frac{T}{T - LK}\left(RY - \frac{K}{T}X\right), \end{aligned} \qquad (4)$$

the feedforward filter should be given by the following equation:

$$\frac{K}{T} = \frac{\omega_{RY}^2}{-\omega^2 + \frac{i\omega\omega_{RY}}{Q_{RY}} + \omega_{RY}^2}\frac{1}{L} \approx -\frac{\omega_{RY}^2}{\omega^2 L}, \qquad (5)$$

at $\omega \gg \omega_{RY}$. However, during our experimental studies, we found that $\sim\omega^{-2}$ dependence is only valid up to $\omega \approx 10\omega_{RY}$. At higher frequencies, the transfer function flattens due to the direct coupling of horizontal motion to our vertical sensors dedicated for RX and RY. Therefore, we fitted the feedforward filter to the transfer function $K/T + \alpha$, where α is a small number on the order of 10^{-2}. The result of the feedforward cancelation is shown in Fig. 2(b).
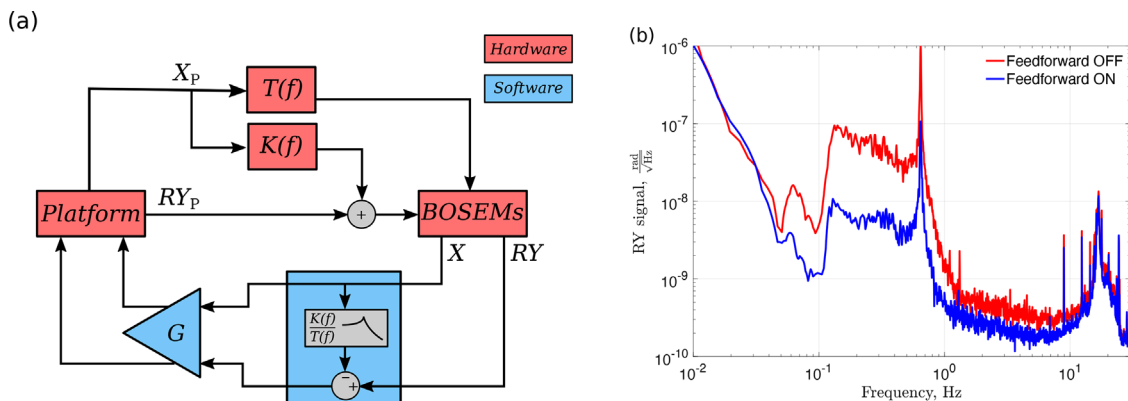

FIG. 2. Feedforward scheme for decoupling translation motion from the tilt readout. (a) A block diagram showing the feedforward scheme to subtract the translational induced tilt motion from the RY measurement. (b) The comparison of the RY signal with (blue) and without (red) feedforward of the X signal.

05 September 2023 08:49:50

Application of the tilt diagonalization and feedforward scheme discussed above enabled stabilization of the platform with six single-input-single-output loops. However, the third strategy aimed to tackle technical issues due to our specific actuated platform.

The upper unity gain frequency was constrained to 10 Hz due to the forest of mechanical resonances of the vacuum chamber and its supporting structure above 14 Hz. The resonances modify the actuation path of the feedback control scheme, and due to the large number of modes, it was implausible to digitally remove the resonances from all degrees of freedom. The bandwidths achieved for the angular modes were 70 mHz–10 Hz for the tilt modes (RX and RY), and 10 mHz–10 Hz for RZ. For the longitudinal degrees of freedom (X and Y), the bandwidth attained was 250 mHz–10 Hz, where the lower unity gain frequency was limited by the cross-couplings of the platform actuation between the X and Y degrees of freedom.

Above 1 Hz, the cross coupling between X and Y degrees of freedom is caused by the imperfect actuation diagonalization matrix and is on the order of 1%. However, the coupling grows significantly toward lower frequencies making the response in X and Y to the excitation in X equal at 40 mHz. The large cross coupling is caused by the tilt-to-horizontal coupling and imperfections of the actuation system: excitation in X also drives RX, resulting in the unpleasant g/ω^2 tilt coupling into the Y degree of freedom. As a consequence, the open loop transfer function of the X degree of freedom is altered when control of Y is simultaneously engaged according to the following equation:

$$H_{\mathrm{mod}} = H + \frac{\beta_x \beta_y G^2}{1 - H}. \tag{6}$$

Here, $H = H_x = H_y$ is the open loop transfer function when stabilization of only one degree of freedom (X or Y) is active, and G is the servo gain as shown in Fig. 2(a). The additional factor is proportional to the cross coupling of the X degree of freedom to Y, β_x, and to the similar coefficient from Y to X, β_y. The additional factor increases the magnitude of the open loop transfer function and makes the closed loop behavior unstable if the lower unity gain frequency of the feedback loop is below 90 mHz for $|\beta_y| = |\beta_x| = 10^{-2}$.

We could reduce the actuation imperfections β_x and β_y down to 0.3% by gain matching the piezo actuators. However, the hysteresis of the actuators causes time-dependent changes to the gains of the piezos depending on the control system. Since the actuation system is non-linear, we cannot reduce the cross coupling coefficients β_x and β_y to the levels below 1% consistently. As a result, we have reduced the control bandwidth in the X and Y degrees of freedom to avoid the instabilities caused by the actuation cross-couplings. However, we expect that the problem of non-linear cross coupling between X and Y degrees of freedom is not present in the suspended active platforms utilized in LIGO.[15]

The performance of the device was limited in part due to the non-linearity of the actuation path, which reduced the desired bandwidth of the feedback control system. However, high gain stabilization of all six degrees of freedom was achieved once correct implementation of the feedforward scheme between X, RY and Y, RX was performed.

For clarity, the error signals (blue) shown in Fig. 3 are a representation of the potential isolation that we have achieved. However, without an independent witness sensor, the reduction shown is only an indication of the platform suppression. The actuation signals (black)

indicate what the motion of the platform would be without the isolation, and the reference traces (red) show the platform motion when no active stabilization of the platform is implemented. The readout noise (magenta) is that of the BOSEMs for each degree of freedom.

Vertical suppression was limited due to the stiff resonant frequency, reducing the bandwidth over which stabilization occurred. Below 1 Hz, the actuation in Z was negligible due to non-inertial sensing, which would result in sensor noise injection. Reduction of the resonant frequency can be achieved by suspending the system from a soft blade spring to reduce the bounce mode, or by increasing the tension on the fiber. The Glasgow group is currently developing higher stress fibers for use in third generation detectors.[36]

For X and Y, the resultant suppression of platform motion was up to two orders of magnitude above 1 Hz and was partially limited by the readout noise. For RX, RY, and RZ, the platform was readout noise limited over a larger frequency band; however, RZ motion before stabilization was already close to readout noise limitation apart from the frequency band between 0.1 and 1 Hz.

The majority of the sensed low frequency motion came from the translational modes, X and Y, and were dominated by the microseismic motion between 0.2 Hz and the 0.62 Hz resonant peaks. The large motion leaked into the other degrees of freedom and can be seen by the red reference traces (no stabilization) in Fig. 3 due to the imperfections of the sensing scheme. Implementation of the feedforward scheme suppressed the coupling into the tilt modes by an order of magnitude in the frequency band from 0.1 to 1 Hz (Fig. 2). Below the bandwidth of the X and Y stabilization (<250 mHz), there is excess motion all degrees of freedom when actuation is implemented. This is a result of the actuation cross couplings of the platform causing the translation motion to leak into the other degrees of freedom. This is shown most clearly in the actuation signal of RZ, which follows the shape of the X and Y spectra.

The high frequency noise in all degrees of freedom above 7 Hz is due to the gain peaking from the control loops, which all have an upper unity gain frequency of 10 Hz apart from the vertical mode.

The error signals in Fig. 3 show the achievable isolation for the current system; however, this is limited by the BOSEM readout noise highlighted by the magenta traces. Further broadband suppression down to the readout noise level was constrained by the limited bandwidth for all degrees of freedom. Improved readout noise would enable the isolation to be solely limited by the bandwidth and the technical issues of our specific actuated platform.

In conclusion, we have demonstrated the viability of stabilizing a six axis platform using a 6D seismometer. The system was operated in high gain with a maximized bandwidth, providing simultaneous control of all six degrees of freedom. We were achievable isolation of more than an order of magnitude at various parts of the frequency band for five of six degrees of freedom. We found the two key principles of the effective control strategy: sensing diagonalization of the tilt modes and decoupling of the horizontal-to-tilt motion. The control techniques are a necessity to diagonalize the degrees of freedom involved in feedback control and to make the overall control system stable.

The system can be further improved in three directions. First, the sensing noise of optical shadow sensors can be improved by two orders of magnitude using interferometric inertial sensors.[37–39] Interferometric sensing has been employed to the system and is currently being optimized to reduce the readout noise.
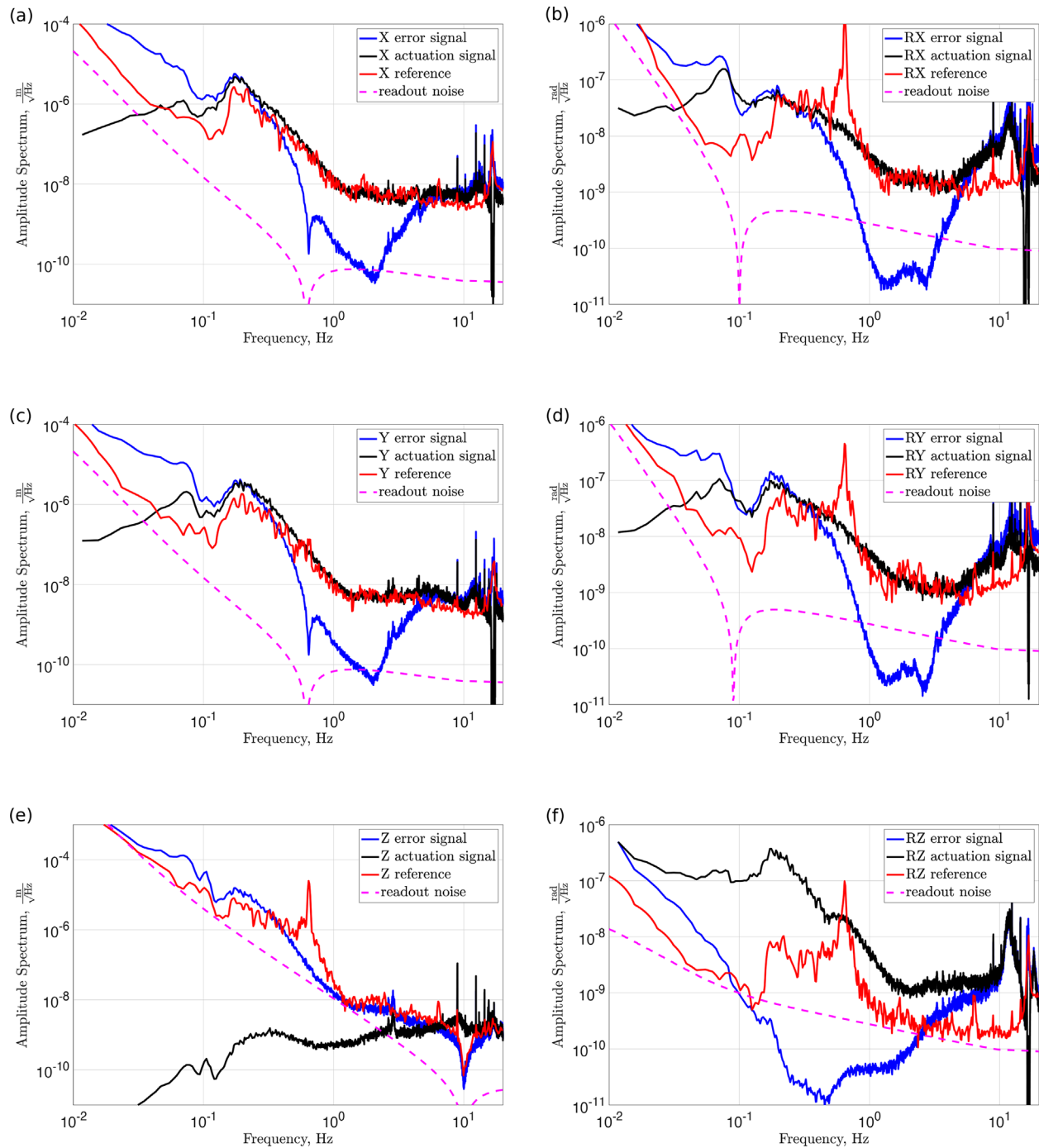
FIG. 3. Performance of the platform stabilization using the 6D seismometer for simultaneous control of all six degrees of freedom. The reference traces (red) indicate the measured platform motion before active stabilization is implemented. The panels represent the (a) X, (b) RX, (c) Y, (d) RY, (e) Z, and (f) RZ degrees of freedom.

Second, the system is susceptible to drift motion for the angular degrees of freedom due to thermal gradients, stress relaxations in the fiber, and in the metal proof mass. We have acquired a fused silica proof mass (discussed in Ref. 35), which has the potential to

reduce the drift motion of the suspended mass due to its low thermal expansion coefficient and lack of plastic deformations. Thermal shielding is also being installed to further isolate the proof mass.

Finally, the actuation of the platform can be improved by suspending it and using coil–magnets actuators similar to the LIGO platforms.[15] As an intermediate step, we may introduce viton sheets to provide passive isolation to damp the high frequency resonant modes of our chamber. This will allow the upper unity gain frequency of the control loops to be increased improving the achievable isolation.

AUTHOR DECLARATIONS
Conflict of Interest

The authors have no conflicts to disclose.

Author Contributions

Amit Singh Ubhi: Data curation (equal); Formal analysis (lead); Investigation (lead); Writing – original draft (lead); Writing – review & editing (lead). **Alan Vernal Cumming:** Resources (equal). **Giles Hammond:** Resources (equal). **Denis Martynov:** Conceptualization (equal); Funding acquisition (equal); Project administration (lead); Supervision (lead); Visualization (equal); Writing – original draft (supporting); Writing – review & editing (supporting). **Leonid G. Prokhorov:** Data curation (equal); Investigation (equal); Methodology (lead); Project administration (supporting). **Sam J. Cooper:** Methodology (equal); Software (equal). **Chiara Di Fronzo:** Software (equal). **John Bryant:** Resources (equal). **David Hoyland:** Resources (equal). **Alexandra Mitchell:** Investigation (supporting). **Jesse van Dongen:** Software (equal). **Conor Mow-Lowry:** Conceptualization (equal); Funding acquisition (equal).

DATA AVAILABILITY

The data that support the findings of this study are available from the corresponding author upon reasonable request.

REFERENCES

[1] J. Aasi, B. P. Abbott, R. Abbott et al., Classical Quantum Gravity **32**, 115012 (2015).

[2] F. Acernese, M. Agathos, K. Agatsuma et al., Classical Quantum Gravity **32**(2015), 024001 (2015).

[3] B. P. Abbott, R. Abbott, T. Abbott et al., Phys. Rev. Lett. **116**, 061102 (2016).

[4] B. P. Abbott, R. Abbott, T. D. Abbott et al., Phys. Rev. X **9**, 031040 (2019).

[5] R. Abbott, T. D. Abbott, S. Abraham et al., Phys. Rev. X **11**, 021053 (2021).

[6] A. H. Nitz, C. D. Capano, S. Kumar et al., Astrophys. J. **922**, 76 (2021).

[7] R. Abbott, T. D. Abbott, S. Abraham et al., Astrophys. J. Lett. **915**, L5 (2021).

[8] B. P. Abbott et al., Phys. Rev. Lett. **116**, 241103 (2016).

[9] B. P. Abbott et al., Phys. Rev. Lett. **119**, 141101 (2017).

[10] R. Abbott, T. D. Abbott, S. Abraham et al., Phys. Rev. Lett. **125**, 101102 (2020).

[11] B. P. Abbott et al., Phys. Rev. Lett. **119**, 161101 (2017).

[12] H. Yu, D. Martynov, S. Vitale et al., Phys. Rev. Lett. **120**, 141102 (2018).

[13] A. Buikema, C. Cahillane, G. L. Mansell et al., Phys. Rev. D **102**, 062003 (2020).

[14] D. V. Martynov, E. D. Hall, B. P. Abbott et al., Phys. Rev. D **93**, 112004 (2016).

[15] F. Matichard, B. Lantz, R. Mittleman et al., Classical Quantum Gravity **32**, 185003 (2015).

[16] F. Matichard, B. Lantz, K. Mason et al., Precis. Eng. **40**, 287 (2015).

[17] F. Matichard, B. Lantz, K. Mason et al., Precis. Eng. **40**, 273 (2015).

[18] K. L. Dooley, L. Barsotti, R. X. Adhikari et al., J. Opt. Soc. Am. A **30**, 2618 (2013).

[19] L. Barsotti, M. Evans, and P. Fritschel, Classical Quantum Gravity **27**, 084026 (2010).

[20] F. Matichard and M. Evans, Bull. Seismol. Soc. Am. **105**, 497 (2015).

[21] F. Matichard, M. Evans, R. Mittleman et al., Rev. Sci. Instrum. **87**, 065002 (2016).

[22] K. Venkateswara, C. Hagedorn, M. Turner et al., Rev. Sci. Instrum. **85**, 015005 (2014).

[23] M. P. Ross, K. Venkateswara, C. Mow-Lowry et al., Classical Quantum Gravity **37**, 185018 (2020).

[24] J. J. McCann, J. Winterflood, L. Ju et al., Rev. Sci. Instrum. **92**, 064503 (2021).

[25] W. Z. Korth, A. Heptonstall, E. D. Hall et al., Classical Quantum Gravity **33**, 035004 (2016).

[26] D. Martynov, N. Brown, E. Nolasco-Martinez et al., Opt. Lett. **44**, 1584 (2019).

[27] See iXblue, https://www.blueseis.net/ for "Rotational seismology;" accessed 28 September 2022.

[28] J. V. van Heijningen, A. Bertolini, and J. F. J. van den Brand, in IEEE Sensors Applications Symposium (SAS), 2018.

[29] C. Collette, F. Nassif, J. Amar et al., Sens. Actuators, A **224**, 72 (2015).

[30] B. Ding, G. Zhao, J. Watchi et al., Sens. Actuators, A **335**, 113398 (2022).

[31] C. M. Mow-Lowry and D. Martynov, Classical Quantum Gravity **36**, 245006 (2019).

[32] A. V. Cumming, A. S. Bell, L. Barsotti et al., Classical Quantum Gravity **29**, 035003 (2012).

[33] A. V. Cumming, B. Sorazu, E. Daw et al., Classical Quantum Gravity **37**, 195019 (2020).

[34] K. A. Strain and B. N. Shapiro, Rev. Sci. Instrum. **83**, 044501 (2012).

[35] A. S. Ubhi, J. Smetana, T. Zhang et al., Classical Quantum Gravity **39**, 015006 (2022).

[36] A. V. Cumming, R. Jones, G. D. Hammond et al., Phys. Rev. Appl. **17**, 024044 (2022).

[37] G. Heinzel, F. G. Cervantes, A. F. G. Marín et al., Opt. Express **18**, 19076 (2010).

[38] O. Gerberding, K.-S. Isleif, M. Mehmet et al., Phys. Rev. Appl. **7**, 024027 (2017).

[39] J. Smetana, R. Walters, S. Bauchinger et al., Phys. Rev. Appl. **18**, 034040 (2022).

05 September 2023 08:49:50